

Efficient $g\text{-C}_3\text{N}_4$ /rGO as a Photo-Electro-Catalyst in a Metal-Free Electro-Fenton Process for the Removal of Levofloxacin

Maryam Rahmani

UNESCO Chair on Water Reuse, School of Chemical Engineering, University of Tehran, Tehran, Iran

Mohammad-Hossein Sarrafzadeh

UNESCO Chair on Water Reuse, School of Chemical Engineering, University of Tehran, Tehran, Iran *Corresponding author: Sarrafzdh@ut.ac.ir

Akram Hosseiniyan

School of Engineering Science, College of Engineering, University of Tehran, Tehran, Iran

Masoud Abdi

School of Chemical Engineering, College of Engineering, University of Tehran, Tehran, Iran

Emerging pollutants significantly impact various ecosystems due to their complex composition, poor biodegradability, and high toxicity. There are several methods for removing these pollutions like advanced oxidation processes, Photo catalyst, and electro chemical processes. The electro-Fenton process combines the advantages of electrochemical and advanced oxidation processes. However, issues such as residual iron remain problematic.

In this project, a composite catalyst of $g\text{-C}_3\text{N}_4$ and rGO, which is completely organic, metal-free, efficient, economical, and green, was utilized as a catalyst in a photo-electro-Fenton-like process to remove the antibiotic levofloxacin. The optimal conditions of this process, including current density, pH, aeration rate, concentration, and composition of the catalyst, were investigated and the optimum amounts of them are 50 mA/cm^2 , $4,400 \text{ ml/min}$, 120 mg/l and $g\text{-C}_3\text{N}_4$ /rGO-1 composite respectively. The performance of the synthesized catalyst was compared with that of pure $g\text{-C}_3\text{N}_4$ in the process. The electro-Fenton process without light exposure and the photocatalyst process were also compared with this process under optimal conditions.

The results demonstrated that the synergistic effect of these processes enhanced levofloxacin removal, achieving a removal percentage of 87% within 90 minutes. The stability of the catalyst was evaluated over four consecutive cycles, showing only a 15% decrease in removal efficiency during the fourth cycle. Additionally, the kinetics of reactions at different conditions were studied, and the reaction rate constants were calculated at a constant temperature.

Keywords: Photo electro-Fenton-like, graphitic carbon nitride, reduced graphene oxide, levofloxacin, emerging pollutant

1. Introduction

Water pollution remains one of the most pressing environmental challenges worldwide. In recent years, the growing diversity and complexity of pollutant compounds have made the release of emerging contaminants a critical concern. Additionally, the intricate nature of various wastewater types has led researchers to characterize their properties using rheological methods. These emerging pollutants, which include unregulated chemical, microbial, and radiological substances, pose a severe threat to ecosystems due to their complex composition, persistence, and high toxicity. Among them, antibiotics are particularly alarming, as they interfere with essential biological processes. The widespread use of antibiotics in modern society has significantly increased their presence in wastewater, establishing them as major emerging pollutants [1–7].

Among the various categories of antibiotics, fluoroquinolones stand out as particularly hazardous in aquatic

environments [8]. These compounds find wide applications in treating infectious diseases of the respiratory tract, genitourinary tract, and skin structures [9]. Levofloxacin (LEV), a third-generation fluoroquinolone, exhibits a broad spectrum of antibacterial effects [10]. Consequently, residual amounts of levofloxacin accumulate in the food chain, posing a global threat to both aquatic and terrestrial ecosystems [11]. The release of such pollutants into the environment, infiltrating different water sources, necessitates enhanced water purification methods for various uses. Removing these substances during water treatment presents more challenges and complexities than treating wastewater containing these pollutants, highlighting the urgent need for innovative wastewater treatment technologies [12].

Advanced oxidation processes (AOPs) offer a promising solution by converting recalcitrant organic pollutants into harmless products such as carbon dioxide and water [13]. Fenton's reagent, a combination of hydrogen peroxide (H_2O_2) and ferrous ion, is one of the most com-

mon methods of advanced oxidation for removing organic pollutants from water. This method boasts non-toxic reactants and products, with hydrogen peroxide decomposing into water and oxygen, making it environmentally friendly [3].

Despite its advantages, the conventional Fenton process has still some challenges such as the requirement for high iron concentrations and the generation of sludge, leading to secondary pollution. The electro-Fenton process, where hydrogen peroxide and ferrous ion are generated electrochemically, addresses some of these issues [14]. However, the problem of metal leaching and the need for secondary purification persist. A promising alternative is the electro-Fenton-like process utilizing metal-free catalysts, which not only outperforms the Fenton-based process at higher pH levels but also eliminates the need for metal reclamation [15].

Graphite carbon nitride ($g\text{-C}_3\text{N}_4$), a photocatalytic nanoparticle composed of organic carbon and nitrogen, presents a notable solution. Its easy and accessible synthesis without metals makes it a prominent candidate for various applications. To harness more visible light, strategies like doping, defect engineering, and compositing with other materials can enhance the band gap and properties of $g\text{-C}_3\text{N}_4$ [16–18]. Studies indicate that graphene-based nanoparticles, with their two-dimensional network and sp^2 conjugation structure, can increase hydrogen peroxide production in the oxygen reduction reaction, a crucial aspect of the electro-Fenton process. Moreover, the extensive conjugated carbon structure in reduced graphene oxide (rGO) provides high electrical conductivity, making this composite suitable for diverse applications, including organic contaminant removal [19, 20].

Despite extensive research on advanced oxidation processes, particularly electro-Fenton, the creation of secondary pollution has hindered their widespread adoption. In this article, we explore a novel approach: the photo-electro-Fenton-like process, utilizing a fully organic catalyst consisting of graphite carbon nitride and reduced graphene oxide. This innovative method is employed to tackle emerging pollutants, particularly focusing on levofloxacin, a resistant antibiotic contaminant.

This study investigates the synthesis and characterization of $g\text{-C}_3\text{N}_4$ /rGO composites and evaluates their performance as photo-electrocatalysts in the photo-electro-Fenton-like process for the efficient removal of levofloxacin. The optimal operational conditions and the stability of the catalyst are also examined to provide an understanding of its potential for practical applications.

2. Experimental Section

2.1. Chemicals and Materials

Graphite flat was purchased from Redoxkala company, and Levofloxacin ($> 99.0 \text{ wt \%}$) was purchased from Tehrandarou company. Sodium sulfate (Na_2SO_4), Sodium thiosulfate ($\text{Na}_2\text{S}_2\text{O}_3$), sulfuric acid (H_2SO_4), Sodium hydroxide (NaOH), and urea were obtained from Merk company. Graphene oxide was obtained from Persian Shimi company. Throughout the experiment, ultra-pure water was used.

2.2. Preparation of Catalysts

$g\text{-C}_3\text{N}_4$ Preparation: Graphitic carbon nitride, a metal-free catalyst, was synthesized from a urea precursor as follows:

15 mg of urea was added to a crucible, and it was completely wrapped with thick aluminum foil. The crucible was then placed in a furnace and heated to 550 °C at a heating rate of 5 °C/min. The synthesis was carried out at this temperature for 3 hours. Finally, after cooling to ambient temperature, carbon nitride was obtained with a conversion rate of 3%.

$g\text{-C}_3\text{N}_4/\text{rGO}$ Preparation: $g\text{-C}_3\text{N}_4/\text{rGO}$ was prepared via a green calcination method [21] using a mixture of urea and graphene oxide. To synthesize this composite with different compositions, the precursors were dissolved in 200 mL of deionized water and sonicated 30 minutes to improve solubility. Next, the solution was stirred thoroughly for 3 hours at 700 rpm and 65 °C, ensuring a homogeneous combination of precursors.

In the next step, the solution was placed in an oven at 70 °C overnight to dry completely. After drying, the precursor was finely ground using a mortar. Finally, composite catalysts with 0.1, 1, and 10 compositions of rGO were synthesized based on the conversion rate of urea. In this article, the name rGO/ $g\text{-C}_3\text{N}_4\text{-}x$ is used to specify the composite catalyst ($x = 0.1, 1, 10$) (Figure 1).

2.3. Characterization Methods

The morphology of the electro-photo catalysts was characterized by Field Emission Scanning Electron Microscopy (FESEM) and Transmission Electron Microscopy (TEM). The crystal phase of the catalysts was analyzed using X-ray crystallography (XRD-PW 1730 $\lambda = 1.54059 \text{ \AA}$: Cu LFF). Fourier Transform Infrared Spectroscopy (FTIR) was used to confirm correct synthesis by identifying the bonding vibrations of the catalysts. Diffuse Reflectance Spectroscopy (DRS) was conducted to calculate the band gap of the nanoparticles. In order to determine the type of photocatalyst and the conduction

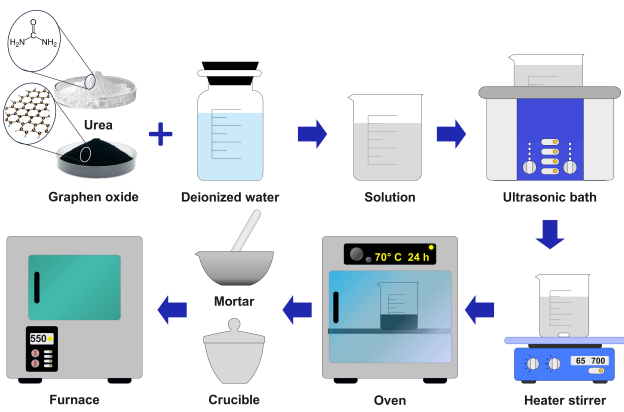


FIG. 1: Synthesis Procedure of $g\text{-C}_3\text{N}_4$ /rGO Composites.

band levels, Mott-Schottky analysis was performed using a Galaxy carbon working electrode, graphite counter electrode, and AgCl/Ag reference electrode. The photoluminescence technique (PL) was conducted to analyze the photoluminescence properties of the catalysts. Additionally, Brunauer-Emmett-Teller (BET) analysis was conducted to determine the specific surface area of the synthesized nanoparticles.

2.4. Photo Electro-Fenton-like Performance Evaluation

The activity of the Photo Electro-Fenton-like (PEFL) system was evaluated by the degradation of levofloxacin. Degradation experiments were conducted in a single-compartment cell with a two-electrode system consisting of graphite anode and cathode electrodes ($2\text{ cm} \times 3\text{ cm} \times 5\text{ mm}$) placed 2 cm apart. Air was bubbled directly into the reaction solution through a pipe positioned near the cathode. Levofloxacin at a concentration of 25 ppm in 250 mL of 0.05 M Na_2SO_4 electrolyte was degraded under various conditions of aeration, current density, initial pH, catalyst concentration, and catalyst composition over 90 minutes at room temperature. The initial pH was adjusted using 0.1 M NaOH and 0.05 M H_2SO_4 .

2.5. Analytical Methods

The concentration of levofloxacin was measured using an ultraviolet spectrometer (Shimadzu/UVmini-1240) at its characteristic peak of 298 nm throughout the experiment. The calibration curve is shown in figure S1. Before the electrocatalytic degradation, the solution containing levofloxacin and catalyst was stirred for 20 minutes in a dark box to investigate the adsorption of $g\text{-C}_3\text{N}_4$ /rGO. Samples of 1 mL were withdrawn and filtered through a

0.22 μm film every 10 minutes. 50 μl of 0.1 M sodium thiosulfate solution were added to quench the remaining hydroxyl radicals. Finally, the concentrations of the initial solution, post-adsorption solution, and PEFL samples were analyzed using the calibration curve.

3. Results and Discussion

3.1. Characterization

The FESEM and TEM images of the nanoparticles are illustrated in Figure 2. As shown in these images, the layers in reduced graphene oxide (Figure 2b) are more separated from each other compared to the layers in graphene oxide (Figure 2a). This increased separation between the layers enhances the accessibility of the active sites of the catalyst and improves mass transfer. The sheet-like structure of graphitic carbon nitride ($g\text{-C}_3\text{N}_4$) is clearly visible in Figure 2c. These sheets are well-defined and exhibit a distinct morphology. When combined with reduced graphene oxide, as seen in the $g\text{-C}_3\text{N}_4$ /rGO-1 composite, the $g\text{-C}_3\text{N}_4$ sheets are placed on the rGO layers, creating a synergistic structure (Figure 2d-f). This arrangement in the composite material is advantageous as it maximizes the contact area between $g\text{-C}_3\text{N}_4$ and rGO, facilitating efficient charge transfer. The improved separation of rGO layers and the strategic placement of $g\text{-C}_3\text{N}_4$ sheets contribute significantly to the enhanced photo-electrocatalytic performance of the composite. This structure is particularly beneficial in the electro-Fenton process for pollutant removal, as it promotes better interaction with the pollutants and efficient degradation. To analyze the crystallographic structure of pure $g\text{-C}_3\text{N}_4$, rGO, and the $g\text{-C}_3\text{N}_4$ /rGO composite, X-ray diffraction (XRD) analysis was performed, and the results are presented in Figure 3.

According to the literature, graphitic carbon nitride ($g\text{-C}_3\text{N}_4$) exhibits two main peaks at around 13° and 27° , corresponding to the tri-s-triazine units and its layered structure, respectively. Reduced graphene oxide (rGO) shows a peak at around 27° and another at approximately 42° , which are associated with its loosely stacked sheets and turbostratic band orientation, respectively [22, 23]. The XRD patterns of the samples align well with those reported in the references.

The presence of the peak at around 42° in the rGO pattern indicates the absence of graphite formation, confirming the successful reduction of graphene oxide. The $g\text{-C}_3\text{N}_4$ /rGO composite exhibits similar XRD peaks as its individual components. However, the intensity of the peaks in the composite is reduced compared to pure $g\text{-C}_3\text{N}_4$. This reduction in peak intensity suggests increased defect formation in the composite catalyst due to the addition of rGO, which disrupts the crystalline order of $g\text{-C}_3\text{N}_4$.

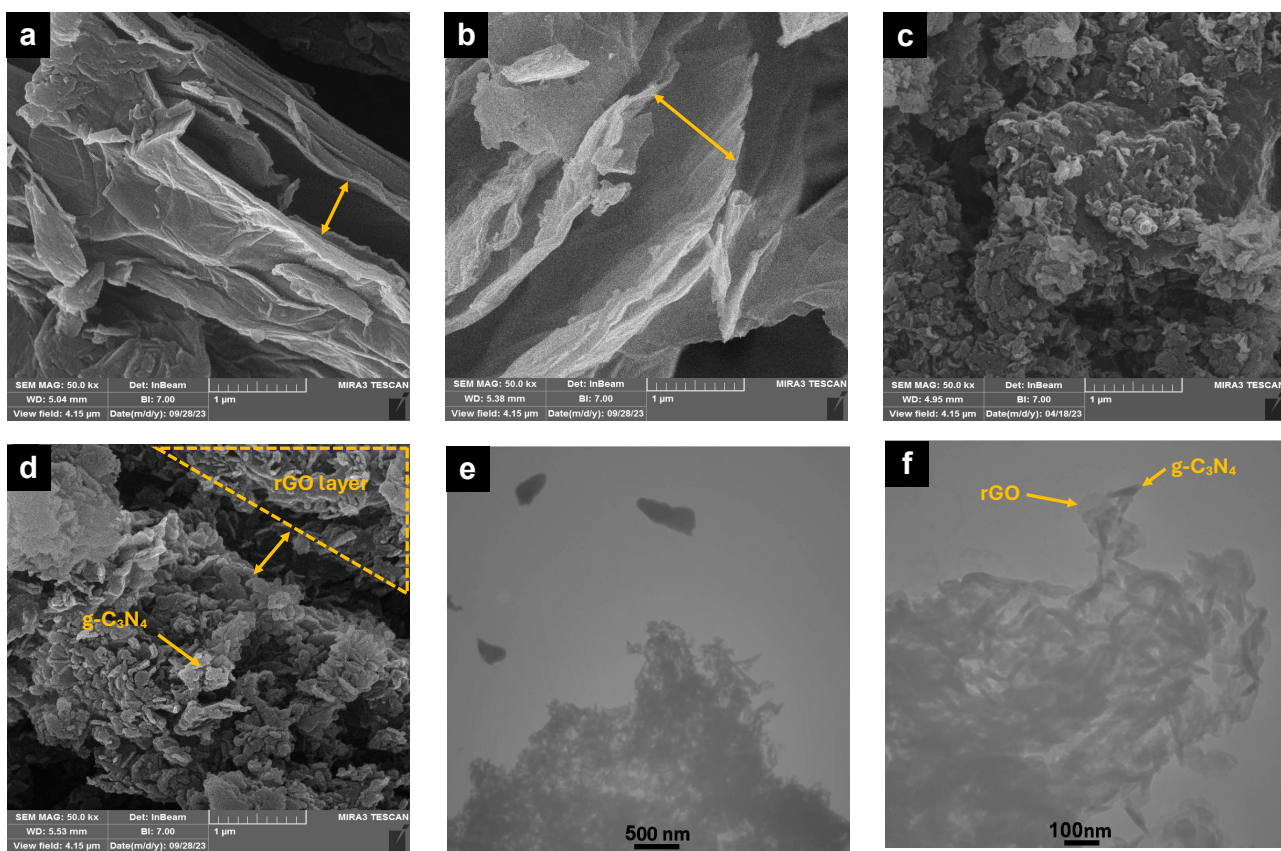


FIG. 2: FESEM images of (a) GO, (b) rGO, (c) $g\text{-C}_3\text{N}_4$, (d) $g\text{-C}_3\text{N}_4$ /rGO composite , TEM images of $g\text{-C}_3\text{N}_4$ /rGO composite in (e) 500 nm and (f) 100 nm.

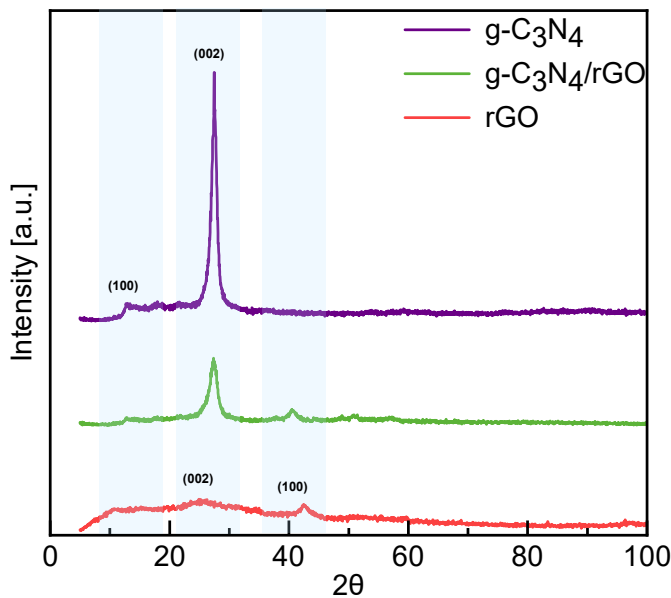


FIG. 3: XRD patterns of pure $g\text{-C}_3\text{N}_4$, $g\text{-C}_3\text{N}_4$ /rGO composite, and rGO.

The incorporation of rGO into the $g\text{-C}_3\text{N}_4$ matrix re-

sults in a more disordered structure, which can enhance the composite's catalytic properties by providing more active sites and improving the overall efficiency of the photo-electrocatalytic process in the electro-Fenton system.

FTIR analysis was employed to investigate the bonds and functional groups present in the synthesized nanoparticles, with the results displayed in Figure 4. A peak in the 3000–3625 cm⁻¹ range corresponds to the OH functional group, which is significantly weakened in rGO due to the reduction process. Additional characteristic peaks include the C=O bond around 1730 cm⁻¹, which indicates the presence of carbonyl groups, and a peak at approximately 1600 cm⁻¹, confirming the graphitic domain and sp² hybridized carbon structure [24]. $g\text{-C}_3\text{N}_4$ exhibits distinct peaks indicative of its chemical structure. Peaks around 3080 and 3200 cm⁻¹ correspond to N-H bonds, representing residual amino groups and absorbed water, respectively. The CN heterojunction peaks, seen in the range of 1200–1640 cm⁻¹, reflect the presence of C-N and C=N bonds within the material. Triazine ring structures are confirmed by peaks at 806 and 735 cm⁻¹, and a peak around 885 cm⁻¹ corresponds to C-H bond vibrations, further confirming the successful synthesis of

g-C₃N₄ [25].

The FTIR spectrum of the *g*-C₃N₄/rGO composite catalyst shows the characteristic peaks of *g*-C₃N₄, affirming its presence in the composite. In addition, a distinct peak related to the C=C bond appears around 980 cm⁻¹, indicating the successful formation of the composite material. This peak signifies the integration of graphene oxide into the graphite carbon nitride matrix, enhancing its structural and electronic properties [23].

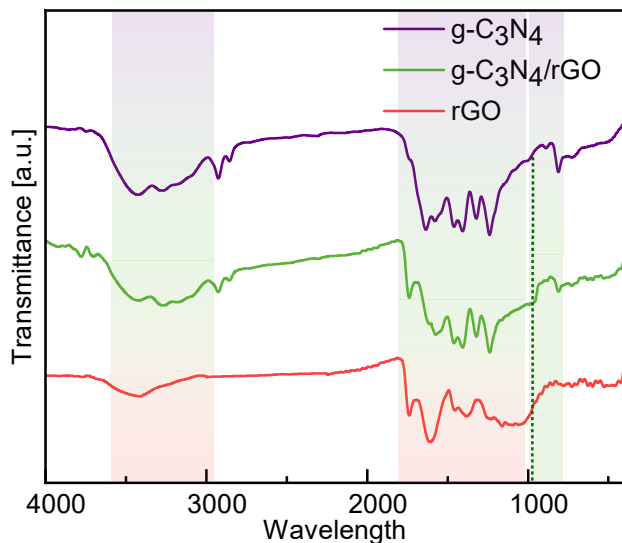


FIG. 4: FTIR spectra of rGO, *g*-C₃N₄, and *g*-C₃N₄/rGO composite catalyst.

The UV-vis diffuse reflectance spectra of pure *g*-C₃N₄, rGO, and the composite catalysts are presented in Figure 5. To determine the value of the energy gap, the Tauc plot, which is a graph of $(\alpha h\nu)^2$ versus photon energy ($h\nu$), was utilized [26]. The energy gap can be calculated in electron volts (eV) using the following equation:

$$E = \frac{hc}{\gamma} \quad \text{or} \quad E = h\nu \quad (1)$$

In these equations, “ α ” represents the absorption coefficient at a specific wavelength, “ h ” is Planck’s constant, “ c ” is the speed of light, “ γ ” is the wavelength of radiation, and “ v ” is the frequency of light. The energy gap values are obtained by drawing a tangent line on the curve at the points where the curve rises with a steep slope in the Tauc plot [26]. According to Figure 5a, rGO has a very low band gap, which can accelerate electron-hole recombination. However, when rGO is added to *g*-C₃N₄, it enhances the performance of *g*-C₃N₄ in the visible light range by reducing its large band gap [23].

The band gap values for *g*-C₃N₄, *g*-C₃N₄/rGO-1, and rGO are 2.89 eV, 2.80 eV, and 1.98 eV respectively. Correspondingly, the activation wavelengths are 429 nm, 443 nm, and 626 nm, respectively.

The valence band (VB) is crucial for determining the photooxidation characteristics of the photocatalyst. The

VB edge potential can be calculated using the energy gap (E_g) and the conduction band (CB) edge potentials. Mott-Schottky plots, with the reference electrode of Li⁺/Li, can be used to determine the CB potential, as the conduction band is approximately equal to the flat band potential [23].

To obtain the conduction band potentials, a tangent line is drawn on the Mott-Schottky plots at the points where the curve rises with a steep slope. Figure 6 shows the Mott-Schottky plots of pure *g*-C₃N₄, rGO, and *g*-C₃N₄/rGO-1. To convert the results of Mott-Schottky plots from the reference electrode of Ag/AgCl to the reference electrode of Li⁺/Li, a value of 3.26 is added as a change in the potential value of the conduction band measured with the Ag/AgCl reference electrode. This shift gives the potential value of the conduction band with the Li⁺/Li reference electrode.

According to the slope of the curves, all photocatalysts are n-type. The potential values of the conduction bands, valence bands, and the energy gaps for the synthesized catalysts are listed in Table I. These values provide insight into the electronic structure and photo-electrocatalytic performance of the *g*-C₃N₄/rGO composite, confirming its potential effectiveness in the electro-Fenton process for removing pollutants.

Photoluminescence (PL) spectroscopic analysis was employed to evaluate the suppression of electron-hole recombination in the synthesized catalysts, pure *g*-C₃N₄, and rGO. The results are presented in Figure 7.

For the *g*-C₃N₄/rGO nanocomposite, the presence of rGO significantly decreases the fluorescence intensity. This reduction in fluorescence is attributed to rGO acting as an electron collector, which facilitates more efficient electron-hole separation in the *g*-C₃N₄/rGO composites. The enhanced separation of charge carriers is expected to improve the overall photo-electrocatalytic performance of the system [27].

Furthermore, the decrease in the peak intensity of the PL spectra indicates an increase in structural defects within the composite [28]. These defects can serve as active sites for catalytic reactions, thereby further enhancing the efficiency of the photo-electrocatalyst. This dual effect of improved charge separation and increased active sites underscores the potential of the *g*-C₃N₄/rGO composite in applications such as the electro-Fenton process for removing emerging pollutants.

Brunauer-Emmett-Teller (BET) analysis was conducted to determine the specific surface area of the synthesized nanoparticles, and the results are presented in Table II. Catalytic reactions are typically surface-dependent, meaning that the reaction rate generally increases with a larger surface area.

However, as shown in Table II, the specific surface areas of the catalysts do not differ significantly. Therefore, it can be concluded that the efficiency of these catalysts is more closely related to their electron transfer mecha-

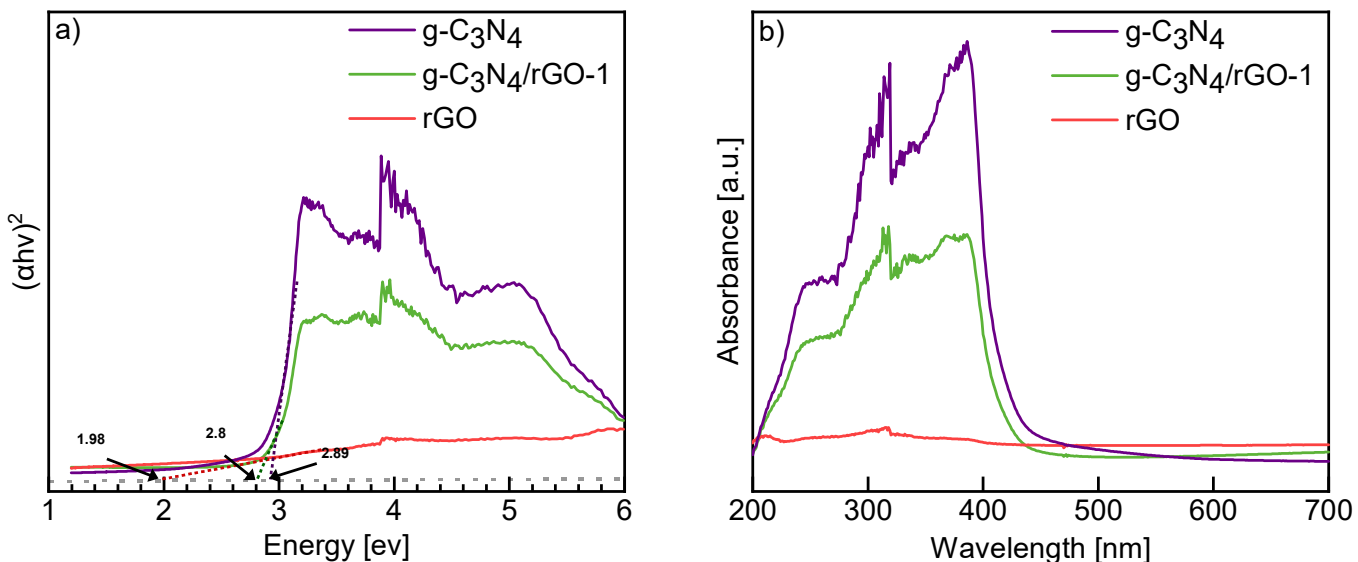


FIG. 5: (a) optimal band gap and (b) absorbance spectroscopy of pure $g\text{-C}_3\text{N}_4$, rGO, and $g\text{-C}_3\text{N}_4/\text{rGO}$ composite.

TABLE I: Conductive band, band gap, and valence band values of pure $g\text{-C}_3\text{N}_4$, rGO, and $g\text{-C}_3\text{N}_4/\text{rGO}$.

Catalyst	Conduction Band ($V_{\text{Ag}/\text{AgCl}}$)	Conduction Band ($V_{\text{Li}^+/\text{Li}}$)	Energy Gap (eV)	Valence Band ($V_{\text{Li}^+/\text{Li}}$)
$g\text{-C}_3\text{N}_4$	-0.46		2.8	2.89
$g\text{-C}_3\text{N}_4/\text{rGO-1}$	-0.2		3.06	2.8
rGO	-0.1		3.16	1.98

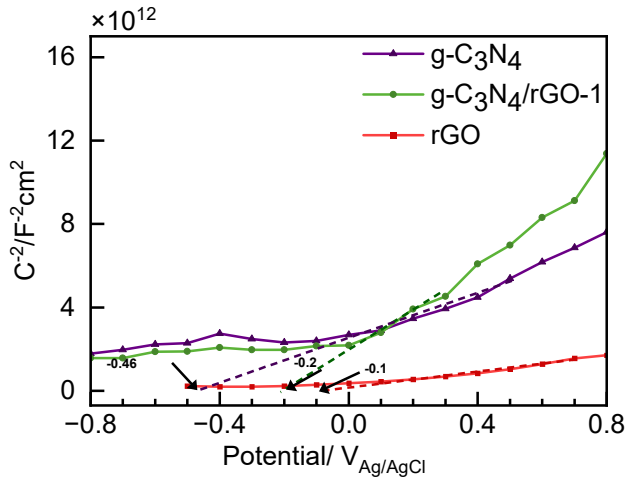


FIG. 6: Mott schottky plot of pure $g\text{-C}_3\text{N}_4$, rGO, and $g\text{-C}_3\text{N}_4/\text{rGO}$ composite.

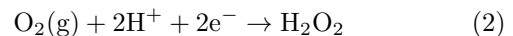
nisms rather than their surface areas. The enhanced performance observed in the $g\text{-C}_3\text{N}_4/\text{rGO}$ composites can be attributed to the improved electron-hole separation and increased structural defects, as indicated by the photoluminescence and Mott-Schottky analyses. These factors collectively enhance the catalytic activity, emphasizing the importance of electronic properties over mere surface area in this context.

4. Effect of Operational Parameters on LEV

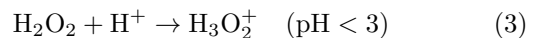
4.1. Effect of pH

The pH of the solution is a critical parameter influencing the progress of reactions in Fenton-based processes. The results of levofloxacin (LEV) removal at different pH levels are presented in Figure 8a. As shown in this figure, the removal efficiency of levofloxacin over 90 minutes of reaction time was 72.87% at pH 2, 87.46% at pH 4, and 86.62% at pH 6, with the highest removal efficiency observed at pH 4.

In electro-Fenton-based processes, acidic pH levels exhibit much higher efficiency compared to basic pH levels [39]. This is because the production of hydrogen peroxide (H_2O_2), which is the primary reactant in the Fenton reaction, increases in acidic conditions according to the following reaction:



However, at pH levels below 3, hydrogen peroxide is converted into oxonium ion through the following reaction [40], which diminishes the efficiency of the Fenton reaction:



Numerous studies have reported that the optimal pH for the electro-Fenton process is between 3 and

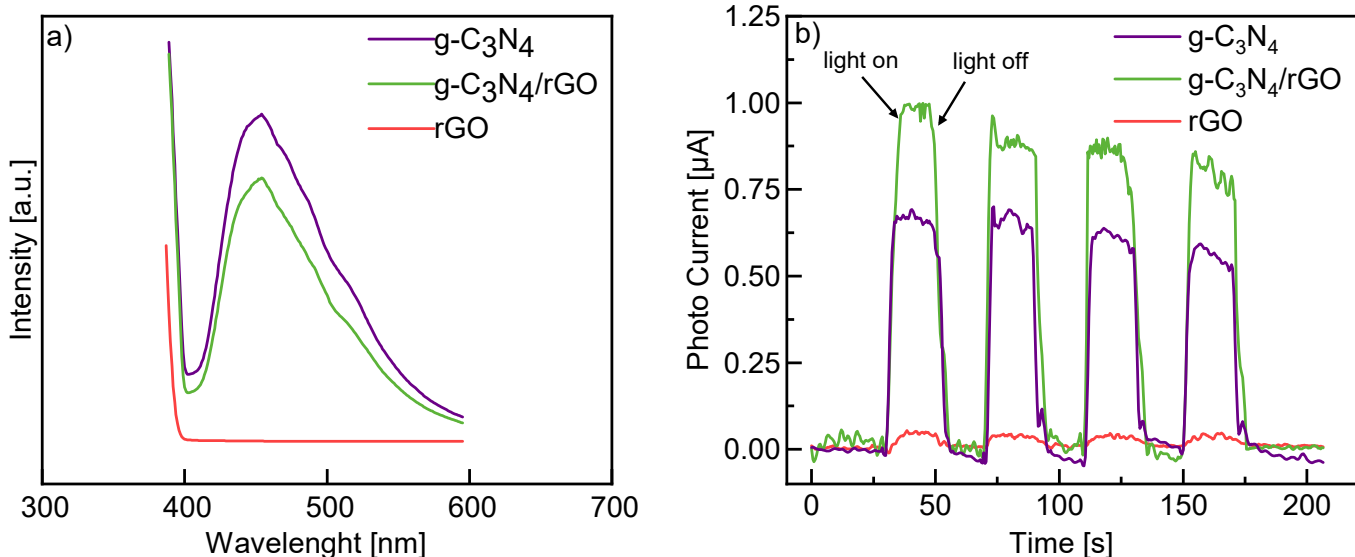


FIG. 7: (a) Photoluminescence spectrum and (b) photocurrent results of pure $g\text{-C}_3\text{N}_4$, rGO, and $g\text{-C}_3\text{N}_4\text{/rGO}$ composites.

TABLE II: Specific surface area of synthesized nanoparticles from BET analysis.

Catalyst	Specific Surface Area in Other Articles (m^2/g)	Specific Surface Area in This Work (m^2/g)	Reference
$g\text{-C}_3\text{N}_4$	142.1	165.8	[29], this work
$g\text{-C}_3\text{N}_4\text{/rGO-0.1}$	-	174.6	this work
$g\text{-C}_3\text{N}_4\text{/rGO-1}$	-	179.7	this work
$g\text{-C}_3\text{N}_4\text{/rGO-10}$	-	168.4	this work

4 [30, 41, 42]. Additionally, the synergistic effect of the electro-Fenton and photocatalytic processes further supports the optimal performance of this process at pH=4. This combination likely enhances the generation of reactive oxygen species and improves the degradation efficiency of pollutants such as levofloxacin.

4.2. Effect of Catalyst Concentration

The amount of catalyst used is another critical parameter in photo-electro-Fenton processes. The catalyst in this process enhances the production rate of hydroxyl radicals by generating electron-hole pairs, thereby increasing pollutant removal [43]. The results of LEV removal with different catalyst concentrations are shown in Figure 8b.

As illustrated in Figure 8b, the optimal catalyst concentration for this process is 120 mg/L, with a removal efficiency of 87.46%. The removal efficiency increases with increasing catalyst concentration from 60 to 120 mg/L but decreases beyond this point. The removal efficiencies of levofloxacin at catalyst concentrations of 60 mg/L and 240 mg/L are 85.98% and 81.00%, respectively, after 90 minutes of reaction.

The decrease in removal efficiency at higher catalyst

concentrations can be attributed to several factors. Excessive catalyst amounts may lead to aggregation, reducing the effective surface area and hindering light penetration. Aggregation can scatter light, decreasing the number of photons reaching the catalyst surface [34]. Additionally, high concentrations of photocatalysts can limit mass transfer and prevent the diffusion of reactants to the active sites on the catalyst surface [44], thus reducing the rate of pollutant removal.

4.3. Effect of Current Density

Since the production of hydrogen peroxide through Reaction 2 is directly dependent on the current intensity, optimizing this parameter is crucial for the photo-electro-Fenton process. In addition, energy consumption costs highlight the importance of optimizing current density. The results of investigating the effect of current density on LEV removal are presented in Figure 8c.

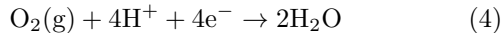
As shown in Figure 8c, the removal efficiency of levofloxacin increased with increasing current density from 30 to 50 mA/cm² during 90 minutes of reaction, reaching a maximum value of 87.46% at 50 mA/cm². Beyond this point, the removal efficiency decreased. The removal efficiencies at 30 mA/cm² and 100 mA/cm² were 57.55%

TABLE III: Comparison of conditions, catalysts, and pollutants in electro-Fenton-based processes.

ID	Contaminant (ppm)	Current/Voltage	Optimum pH	Catalyst	Volume (mL)	Aeration (mL/min)	Configuration	Removal (%)	Reference
1	Phenol (50)	0.8 V	4	FeOx/NHPC750	30	20 O ₂	2-electrode	100%	[30]
2	Sulfamethoxazole (20)	0.6 V	3	FeSO ₄ ·7H ₂ O	25	0.65 mmol H ₂ O ₂	2-electrode	100%	[31]
3	Rhodamine B (50)	0.9 V	3	MOF(2Fe/Co)/CA	100	300 Air	3-electrode	100%	[32]
4	Ciprofloxacin (50)	30 mA/cm ²	3	FeSO ₄	50	100 O ₂	3-electrode	100%	[33]
5	Phenol (50)	3 V	3–4	<i>g</i> -C ₃ N ₄	70	50 O ₂	2-electrode	<85%	[34]
6	Tetracycline (20)	40 mA/cm ²	3	Cu-doped Fe@Fe ₂ O ₃	400	100 Air	2-electrode	~90%	[35]
7	Norfloxacin (10–25)	9 mA	3.5–4	Fe	—	200 Air	2-electrode	>99%	[36]
8	Tetracycline (5–30)	100 mA/cm ²	5.56	UiO-66-SO ₃ H/Fe	100	500 Air	2-electrode	90.1%	[37]
9	Levofloxacin	0.45 V	7.3	NAVO ₃	—	2 mmol/L H ₂ O ₂	3-electrode	80%	[38]
10	Levofloxacin (25)	50 mA/cm ²	4	<i>g</i> -C ₃ N ₄ /rGO	200	400 Air	2-electrode	~87%	This study

and 84.92%, respectively. Although the percentage of removal at a current density of 100 mA/cm² was the highest after 30 minutes, the significant increase in energy consumption at this current density makes it economically unfeasible.

The decrease in efficiency at current densities above 50 mA/cm² can be attributed to the conversion of hydrogen peroxide and oxygen to water at high current densities, as described by the following reaction [42]:



Additionally, high current densities can lead to the excessive production of active species such as hydroxyl radicals on the electrode surface. Although these species are crucial for pollutant removal, their overproduction can stimulate side reactions, reducing the overall efficiency. Furthermore, increasing current intensity raises the likelihood of oxygen production at the anode and hydrogen production at the cathode. This shift decreases the production of hydrogen peroxide, thereby lowering the process efficiency [45].

4.4. Effect of Aeration

One of the key advantages of electro-Fenton-based processes is the production of hydrogen peroxide via electrochemical methods, facilitated by aeration at the cathode during the process [46]. Therefore, it is essential to optimize the amount of aeration to enhance system performance while minimizing economic costs. The results of the tests determining the optimal aeration level for this process are presented in Figure 8d.

As shown in this figure, increasing the aeration rate from 0.2 L/min (with a removal efficiency of 84.99%) to 0.4 L/min improves the system's performance, achieving the highest removal efficiency of 87.46%. Beyond this point, the removal efficiency remains almost constant, reaching 87.55% at an aeration rate of 0.6 L/min during 90 minutes of reaction.

Increasing the aeration rate to the optimal level enhances the amount of dissolved oxygen in the water, thereby maximizing H₂O₂ production. This increase in H₂O₂ production is directly related to the higher gen-

eration of hydroxyl radicals, which are crucial for pollutant removal. However, beyond the optimal aeration rate, the process efficiency plateaus. This plateau occurs because the dissolved oxygen in the water reaches saturation [45]. Furthermore, excess oxygen bubbles increase the resistance of the solution and the likelihood of side reactions, such as hydrogen evolution, which can reduce overall process efficiency [47].

By determining the optimal aeration point, we can improve the efficiency of the electro-Fenton process for levofloxacin removal, ensuring effective treatment of wastewater while keeping economic costs in check.

4.5. Effect of Catalyst Composition

Three different combinations of catalysts were synthesized to investigate the optimal composition of *g*-C₃N₄/rGO for the efficient removal of LEV using the photo-electro-Fenton method. The results of the efficiency of the removal of levofloxacin using these photocatalysts are presented in Figure 8e.

As shown in Figure 8e, the pollutant removal efficiency increases with the increase of rGO in the catalyst up to 1%, after which the removal efficiency decreases. The synthesized catalyst exhibited the highest pollutant removal rate of 87.46% at a composition of 1% rGO. In this composition, the synergistic effect of the *g*-C₃N₄ photocatalyst and the rGO electrocatalyst likely enhances performance. The removal efficiencies for the compositions of 0.1% and 10% rGO were 85.07% and 84.38%, respectively.

At very high concentrations of rGO, aggregation and masking of the active surface area are the primary causes of the diminished overall efficiency of the catalyst [48]. Furthermore, the BET results confirm the aggregation at very high concentrations of rGO.

By optimizing the composition of the catalyst, particularly the ratio of *g*-C₃N₄ to rGO, we can significantly improve the efficiency of the electro-Fenton process for the removal of levofloxacin, ensuring effective wastewater treatment.

4.6. Determination of Reaction Kinetics

Determining the degradation kinetics is crucial for designing effective treatment systems for wastewater. The degradation kinetics of levofloxacin were modeled using a first-order reaction, which accurately predicted levofloxacin concentrations over time with very low error, consistent with the experimental data. The reaction kinetics are described by the following equation:

$$\ln \left(\frac{C}{C_0} \right) = -Kt \quad (5)$$

Where C is the concentration of levofloxacin at time t , C_0 is the initial concentration of levofloxacin, and K is the reaction rate constant.

The reaction rate constants were measured under different conditions and presented in Figure 8. The results provide valuable insight into optimizing the process conditions to achieve maximum efficiency in levofloxacin degradation.

4.7. Comparison of Photocatalyst, Electro-Fenton-like, and Photo-Electro-Fenton-like Processes

To investigate the effects of photocatalytic and electrocatalytic processes and their combination on LEV removal, the best catalyst composition was used under optimal conditions determined for these three processes. The results are shown in Figure 8f.

As depicted in Figure 8f, both photocatalyst and electro-Fenton-like processes are capable of removing levofloxacin. However, the synergistic effect of combining these processes significantly enhances the performance of the photo-electro-Fenton-like process.

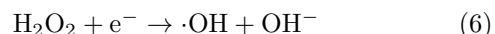
The removal efficiencies for the photocatalyst, electro-Fenton-like, and photo-electro-Fenton-like processes are 43.77%, 80.15%, and 87.46%, respectively. These results clearly demonstrate that the combination of photocatalytic and Fenton-based processes leads to a higher efficacy in pollutant removal. The synergistic effect arises from the enhanced production of reactive oxygen species (ROS) and improved electron-hole separation [49], which accelerate the degradation of levofloxacin.

By leveraging the strengths of both photocatalytic and electro-Fenton-like processes, the photo-electro-Fenton-like process offers a more efficient and effective method for wastewater treatment, achieving higher removal rates of emerging pollutants such as levofloxacin.

4.8. Comparison of $g\text{-C}_3\text{N}_4$ and $g\text{-C}_3\text{N}_4/\text{rGO}$ efficiency in electro fenton process

To evaluate the synthesized catalyst, the efficiency of the photo-electro-Fenton process for LEV removal with the composite catalyst was compared to the pure $g\text{-C}_3\text{N}_4$ catalyst. The results of this comparison are shown in Figure 9.

As seen in Figure 9, the heterojunction of $g\text{-C}_3\text{N}_4$ rGO enhances the separation of photo-generated electron-hole pairs [27], thereby increasing the progress of the following reaction and overall efficiency:



The $g\text{-C}_3\text{N}_4/\text{rGO}$ composite generates active species, including $\cdot\text{OH}$, O_2^- , and h^+ , through the photoelectric synergy between rGO and $g\text{-C}_3\text{N}_4$ [50]. This significantly accelerates the degradation efficiency of levofloxacin.

The efficacy of pollutant removal in the process using the $g\text{-C}_3\text{N}_4$ catalyst and the $g\text{-C}_3\text{N}_4/\text{rGO}$ composite was 80.42% and 87.46%, respectively. These results indicate that the $g\text{-C}_3\text{N}_4/\text{rGO}-1$ composite catalyst is more effective than pure $g\text{-C}_3\text{N}_4$, highlighting the benefits of combining $g\text{-C}_3\text{N}_4$ with rGO for enhanced photo-electro-Fenton performance.

5. Conclusion

In this project, $g\text{-C}_3\text{N}_4$ and rGO composite was synthesized from graphene oxide and urea precursors. To ensure the correct synthesis of the catalysts, various analyses such as FE-SEM, XRD, FTIR, PL, and Mott-Schottky were utilized. These composites were then employed as the main catalysts in a photo-electro-Fenton-like system to investigate their performance in removing levofloxacin, a model antibiotic. The optimal conditions for the process were determined to be: current density = 50 mA/cm², aeration rate = 0.4 L/min, pH = 4, and 120 mg/L of the 1% reduced graphene oxide composite catalyst. The performance of the process was compared with systems containing pure $g\text{-C}_3\text{N}_4$ catalysts. Furthermore, the photocatalytic process, electro-Fenton-like process, and photo-electro-Fenton-like process, all using $g\text{-C}_3\text{N}_4/\text{rGO}$ as their main catalyst, were compared. Additionally, the reaction kinetics was studied under different conditions. The kinetics was found to follow a first-order reaction model.

Table III provides a comparison of the conditions, catalysts, and pollutants used in electro-Fenton-based processes from this study and those reported in other articles. This comparison serves as a valuable roadmap for future research, highlighting the advancements made and identifying areas for further exploration.

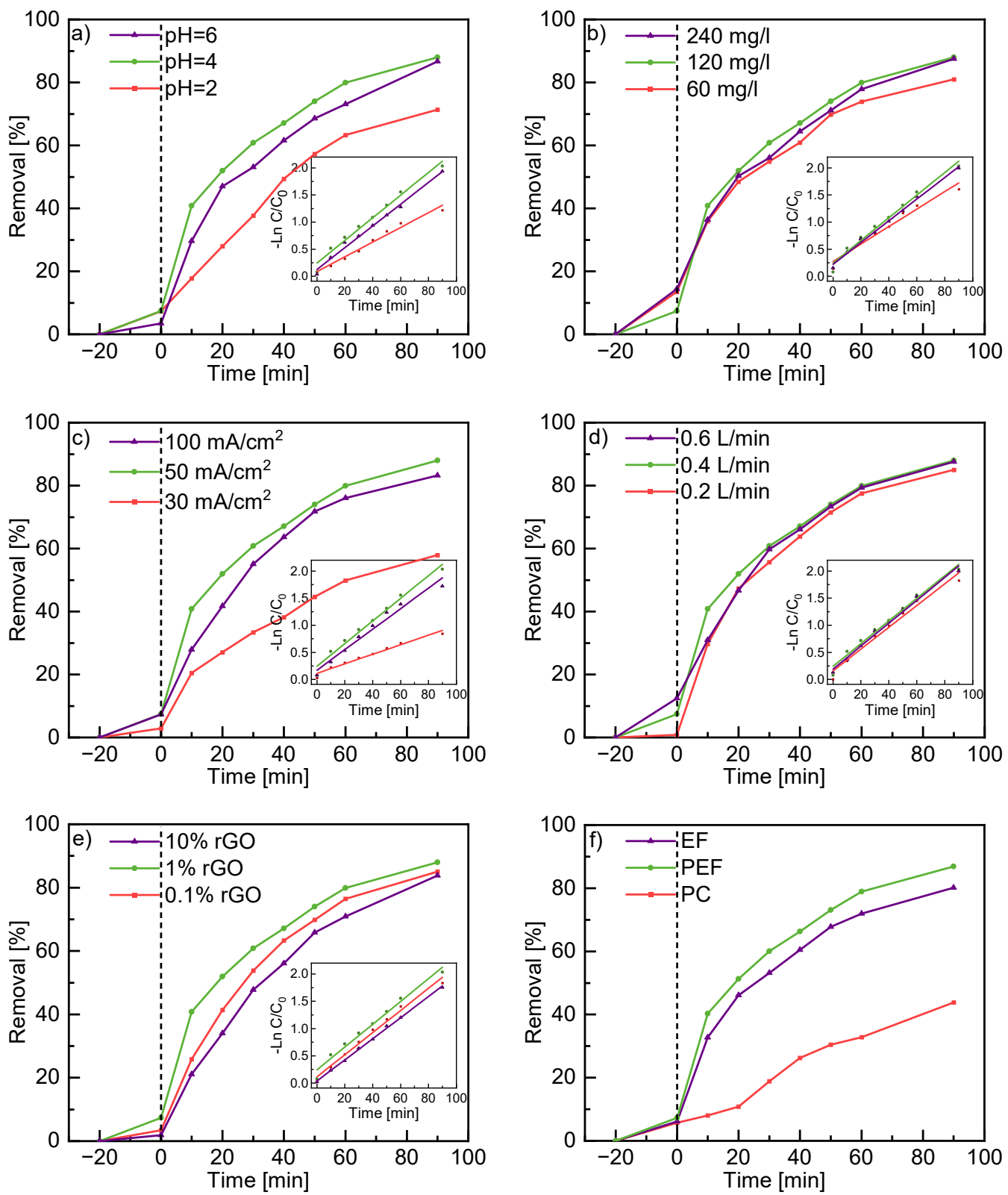


FIG. 8: Effect of (a) pH value, (b) Catalyst Concentration, (c) Current Density, (d) Aeration, and (e) Catalyst Composition on the LEV removal in the Photo-Electro-Fenton-like process and (f) Comparison of Photo catalyst, Electro Fenton and Photo Electro Fenton.

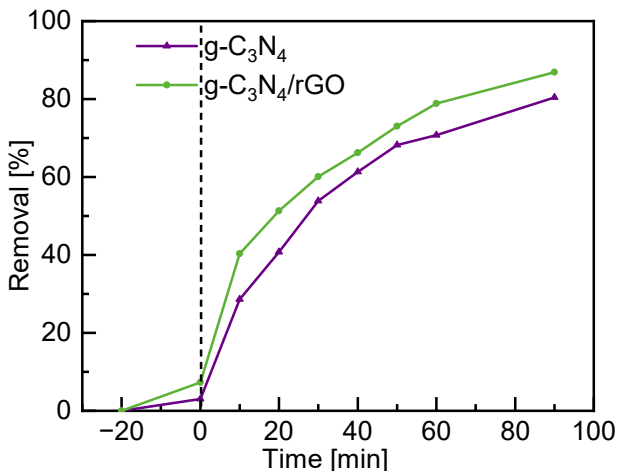


FIG. 9: Comparison of $g\text{-C}_3\text{N}_4$ and $g\text{-C}_3\text{N}_4/\text{rGO}$ -1.

References

- [1] D. Liu, K. Li, M. Li, Z. Wang, M. Shan, and Y. Zhang, "Moderately Crystalline Azine-Linked Covalent Organic Framework Membrane for Ultrafast Molecular Sieving," *ACS Applied Materials & Interfaces*, vol. 13, pp. 37775–37784, Aug. 2021.
- [2] A. Esmaeeli and M.-H. Sarrafzadeh, "Reducing freshwater consumption in pulp and paper industries using pinch analysis and mathematical optimization," *Journal of Water Process Engineering*, vol. 53, p. 103646, July 2023.
- [3] L. Qiu, Z. Dong, H. Sun, H. Li, and C.-C. Chang, "Emerging Pollutants – Part I: Occurrence, Fate and Transport," *Water Environment Research*, vol. 88, pp. 1855–1875, Oct. 2016.
- [4] S. Li, P. L. Show, H. H. Ngo, and S.-H. Ho, "Algae-mediated antibiotic wastewater treatment: A critical review," *Environmental Science and Ecotechnology*, vol. 9, p. 100145, Jan. 2022.
- [5] E. Nikoumanesh and R. Poling-Skutvik, "The effect of thixotropy on the yield transition in reversible, colloidal gels," *The Journal of Chemical Physics*, vol. 159, p. 044905, July 2023.
- [6] E. Nikoumanesh, C. J. M. Jouaneh, and R. Poling-Skutvik, "Elucidating the role of physicochemical interactions on gel rheology," *Soft Matter*, vol. 20, no. 36, pp. 7094–7102, 2024.
- [7] I. Seyssieq, J.-H. Ferrasse, and N. Roche, "State-of-the-art: Rheological characterisation of wastewater treatment sludge," *Biochemical Engineering Journal*, vol. 16, pp. 41–56, Oct. 2003.
- [8] L. Saya, V. Malik, D. Gautam, G. Gambhir, Balendra, W. R. Singh, and S. Hooda, "A comprehensive review on recent advances toward sequestration of levofloxacin antibiotic from wastewater," Mar. 2022.
- [9] K. F. Croom and K. L. Goa, "Levofloxacin," *Drugs*, vol. 63, no. 24, pp. 2769–2802, 2003.
- [10] K. F. Croom, K. L. Goa, J. M. Blondeau, D. R. P. Guay, J. A. Ramirez, and K. A. Rodvold, "ADIS DRUG EVALUATION Levofloxacin A Review of its Use in the Treatment of Bacterial Infections in the United States," 2003.
- [11] J. Fick, . Hanna, S. S. So"derstro, S. So"derstro"m, R. H. Lindberg, C. Phan, and D. G. J. Larsson{, "Pharmaceuticals and Personal Care Products in the Environment CONTAMINATION OF SURFACE, GROUND, AND DRINKING WATER FROM PHARMACEUTICAL PRODUCTION,"
- [12] F. Laghrib, M. Bakasse, S. Lahrich, and M. A. E. Mhammedi, "Advanced oxidation processes: Photo-electro-Fenton remediation process for wastewater contaminated by organic azo dyes," 2021.
- [13] P.-J. Lin, C.-H. Yeh, and J.-C. Jiang, "Theoretical insight into hydroxyl production via H_2O_2 decomposition over the Fe_3O_4 (311) surface," *RSC Advances*, vol. 11, no. 57, pp. 36257–36264, 2021.
- [14] I. Sirés and E. Brillas, "Electro-Fenton process: Fundamentals and reactivity," in *Handbook of Environmental Chemistry*, vol. 61, pp. 1–28, Springer Verlag, 2018.
- [15] Y. Zhu, W. Fan, W. Feng, Y. Wang, S. Liu, Z. Dong, and X. Li, "A critical review on metal complexes removal from water using methods based on Fenton-like reactions: Analysis and comparison of methods and mechanisms," *Journal of Hazardous Materials*, vol. 414, p. 125517, July 2021.
- [16] J. Wen, J. Xie, X. Chen, and X. Li, "A review on $g\text{-C}_3\text{N}_4$ -based photocatalysts," *Applied Surface Science*, vol. 391, pp. 72–123, Jan. 2017.
- [17] M. Rezaei-DashtArzhandi, M. H. Sarrafzadeh, P. S. Goh, W. J. Lau, A. F. Ismail, and M. A. Mohamed, "Development of novel thin film nanocomposite forward osmosis membranes containing halloysite/graphitic carbon nitride nanoparticles towards enhanced desalination performance," *Desalination*, vol. 447, pp. 18–28, Dec. 2018.
- [18] Z. Sun, X. Zhang, X. Dong, X. Liu, Y. Tan, F. Yuan, S. Zheng, and C. Li, "Hierarchical assembly of highly efficient visible-light-driven $\text{Ag}/g\text{-C}_3\text{N}_4/\text{kaolinite}$ composite photocatalyst for the degradation of ibuprofen," *Journal of Materomics*, vol. 6, pp. 582–592, Sept. 2020.
- [19] H. W. Kim, M. B. Ross, N. Kornienko, L. Zhang, J. Guo, P. Yang, and B. D. McCloskey, "Efficient hydrogen peroxide generation using reduced graphene oxide-based oxygen reduction electrocatalysts," *Nature Catalysis*, vol. 1, pp. 282–290, Apr. 2018.
- [20] Y. Li, H. Zhang, P. Liu, D. Wang, Y. Li, and H. Zhao, "Cross-linked $g\text{-C}_3\text{N}_4/\text{rGO}$ nanocomposites with tunable band structure and enhanced visible light photocatalytic activity," *Small*, vol. 9, pp. 3336–3344, Oct. 2013.
- [21] B. Yuan, J. Wei, T. Hu, H. Yao, Z. Jiang, Z. Fang, and Z. Chu, "Simple synthesis of $g\text{-C}_3\text{N}_4/\text{rGO}$ hybrid catalyst for the photocatalytic degradation of rhodamine B," *Chinese Journal of Catalysis*, vol. 36, pp. 1009–1016, July 2015.
- [22] N. M. S. Hidayah, W.-W. Liu, C.-W. Lai, N. Z. Noriman, C.-S. Khe, U. Hashim, and H. C. Lee, "Comparison on graphite, graphene oxide and reduced graphene oxide: Synthesis and characterization," p. 150002, 2017.
- [23] E. Lökcü, N. Kaçar, M. Çayırılı, R. C. Özden, and M. Anik, "Photoassisted Charging of Li-Ion Oxygen Batteries Using $g\text{-C}_3\text{N}_4/\text{rGO}$ Nanocomposite Photocatalysts," *ACS Applied Materials & Interfaces*, vol. 14, pp. 34583–34592, Aug. 2022.
- [24] F. Y. Ban, S. R. Majid, N. M. Huang, and H. N. Lim, "Graphene Oxide and Its Electrochemical Performance," *International Journal of Electrochemical Science*, vol. 7, no. 5, pp. 4345–4351, 2012.

- [25] S. Samanta, S. Martha, and K. Parida, "Facile Synthesis of Au/g-C₃N₄ Nanocomposites: An Inorganic/Organic Hybrid Plasmonic Photocatalyst with Enhanced Hydrogen Gas Evolution Under Visible-Light Irradiation," *ChemCatChem*, vol. 6, pp. 1453–1462, May 2014.
- [26] X.-j. Wang, Q. Wang, F.-t. Li, W.-y. Yang, Y. Zhao, Y.-j. Hao, and S.-j. Liu, "Novel BiOCl–C3N4 heterojunction photocatalysts: In situ preparation via an ionic-liquid-assisted solvent-thermal route and their visible-light photocatalytic activities," *Chemical Engineering Journal*, vol. 234, pp. 361–371, Dec. 2013.
- [27] X. Cai, H. Liu, L. Zhi, H. Wen, A. Yu, L. Li, F. Chen, and B. Wang, "A g-C₃N₄/rGO nanocomposite as a highly efficient metal-free photocatalyst for direct C–H arylation under visible light irradiation," *RSC Adv.*, vol. 7, no. 73, pp. 46132–46138, 2017.
- [28] P. N. Thang, L. X. Hung, D. N. Thuan, N. H. Yen, N. T. T. Hien, V. T. H. Hanh, N. C. Khang, J. Laverdant, and P. T. Nga, "Temperature-dependent Raman investigation and photoluminescence of graphene quantum dots with and without nitrogen-doping," *Journal of Materials Science*, vol. 56, pp. 4979–4990, Mar. 2021.
- [29] J. Yang, X. Zhang, C. Xie, J. Long, Y. Wang, L. Wei, and X. Yang, "Preparation of g-C3N4 with High Specific Surface Area and Photocatalytic Stability," *Journal of Electronic Materials*, vol. 50, pp. 1067–1074, Mar. 2021.
- [30] P. Cao, X. Quan, K. Zhao, S. Chen, H. Yu, and J. Niu, "Selective electrochemical H₂O₂ generation and activation on a bifunctional catalyst for heterogeneous electro-Fenton catalysis," *Journal of Hazardous Materials*, vol. 382, Jan. 2020.
- [31] X. Qin, K. Wang, P. Cao, Y. Su, S. Chen, H. Yu, and X. Quan, "Highly efficient electro-Fenton process on hollow porous carbon spheres enabled by enhanced H₂O₂ production and Fe²⁺ regeneration," *Journal of Hazardous Materials*, vol. 446, Mar. 2023.
- [32] H. Zhao, Y. Chen, Q. Peng, Q. Wang, and G. Zhao, "Catalytic activity of MOF(2Fe/Co)/carbon aerogel for improving H₂O₂ and [rad] OH generation in solar photo-electro-Fenton process," *Applied Catalysis B: Environmental*, vol. 203, pp. 127–137, Apr. 2017.
- [33] Y. Wang, J. Chen, J. Gao, H. Meng, S. Chai, Y. Jian, L. Shi, Y. Wang, and C. He, "Selective electrochemical H₂O₂ generation on the graphene aerogel for efficient electro-Fenton degradation of ciprofloxacin," *Separation and Purification Technology*, vol. 272, Oct. 2021.
- [34] D. Yue, X. Qian, M. Kan, M. Fang, J. Jia, X. Yang, and Y. Zhao, "A metal-free visible light active photo-electro-Fenton-like cell for organic pollutants degradation," *Applied Catalysis B: Environmental*, vol. 229, pp. 211–217, Aug. 2018.
- [35] H. Guo, C.-G. Niu, L. Zhang, X.-J. Wen, C. Liang, X.-G. Zhang, D.-L. Guan, N. Tang, and G.-M. Zeng, "Construction of Direct Z-Scheme AgI/Bi₂Sn₂O₇ Nanojunction System with Enhanced Photocatalytic Activity: Accelerated Interfacial Charge Transfer Induced Efficient Cr(VI) Reduction, Tetracycline Degradation and *Escherichia coli* Inactivation," *ACS Sustainable Chemistry & Engineering*, vol. 6, pp. 8003–8018, June 2018.
- [36] Y. Liu, C. Gao, L. Liu, T. Yu, and Y. Li, "Improved degradation of tetracycline, norfloxacin and methyl orange wastewater treatment with dual catalytic electrode assisted self-sustained Fe²⁺ electro-Fenton system: Regulatory factors, mechanisms and pathways," *Separation and Purification Technology*, vol. 284, Feb. 2022.
- [37] L. Qin, Q. Sun, C. Lai, S. Liu, X. Qin, W. Chen, Y. Fu, X. Zhou, F. Xu, and D. Ma, "Sulfonic acid metal-organic frameworks derived iron-doped carbon as novel heterogeneous electro-Fenton catalysts for the degradation of tetracycline: Performance and mechanism investigation," *Chemical Engineering Journal*, vol. 474, Oct. 2023.
- [38] J. Liang, Y. Hou, H. Zhu, J. Xiong, W. Huang, Z. Yu, and S. Wang, "Levofloxacin degradation performance and mechanism in the novel electro-Fenton system constructed with vanadium oxide electrodes under neutral pH," *Chemical Engineering Journal*, vol. 433, Apr. 2022.
- [39] M. Kiranşan, "An Overview of Applications of the Electro-Fenton (e-/H₂O₂/Fe²⁺) Oxidation Processes: Degradation of Acid and Basic Dyes in the Industrial Wastewaters," *Russian Journal of Physical Chemistry A*, vol. 97, pp. 883–893, May 2023.
- [40] M. Zhou, Q. Yu, L. Lei, and G. Barton, "Electro-Fenton method for the removal of methyl red in an efficient electrochemical system," *Separation and Purification Technology*, vol. 57, pp. 380–387, Oct. 2007.
- [41] M. hui Zhang, H. Dong, L. Zhao, D. xi Wang, and D. Meng, "A review on Fenton process for organic wastewater treatment based on optimization perspective," June 2019.
- [42] P. V. Nidheesh and R. Gandhimathi, "Trends in electro-Fenton process for water and wastewater treatment: An overview," *Desalination*, vol. 299, pp. 1–15, Aug. 2012.
- [43] A. Shokri and M. S. Fard, "A critical review in Fenton-like approach for the removal of pollutants in the aqueous environment," *Environmental Challenges*, vol. 7, p. 100534, Apr. 2022.
- [44] M. Náfrádi, G. Veréb, D. S. Firak, and T. Alapi, "Photocatalysis: Introduction, Mechanism, and Effective Parameters," pp. 3–31, 2022.
- [45] H. He and Z. Zhou, "Electro-Fenton process for water and wastewater treatment," *Critical Reviews in Environmental Science and Technology*, vol. 47, pp. 2100–2131, Nov. 2017.
- [46] Y. Yao, Y. Pan, Y. Yu, Z. Yu, L. Lai, F. Liu, L. Wei, and Y. Chen, "Bifunctional catalysts for heterogeneous electro-Fenton processes: A review," *Environmental Chemistry Letters*, vol. 20, pp. 3837–3859, Dec. 2022.
- [47] L. Zhou, M. Zhou, C. Zhang, Y. Jiang, Z. Bi, and J. Yang, "Electro-Fenton degradation of p-nitrophenol using the anodized graphite felts," *Chemical Engineering Journal*, vol. 233, pp. 185–192, Nov. 2013.
- [48] M. Kasinathan, S. Thiripuranthagan, and A. Sivakumar, "Fabrication of metal-free 2D/2D g-C3N4/rGO composite towards the degradation of harmful organics," *Optik*, vol. 219, p. 165023, Oct. 2020.
- [49] C. Dong, M. Xing, and J. Zhang, "Recent Progress of Photocatalytic Fenton-Like Process for Environmental Remediation," *Frontiers in Environmental Chemistry*, vol. 1, Sept. 2020.
- [50] C. Zhao, H. Sun, C. Li, M. Wang, J. Wu, M. Chen, S. Jiang, T. Niu, and D. Liu, "Facile Synthesis of 3D Interconnected Porous g-C3N4/rGO Composite for Hydrogen Production and Dye Elimination," *Catalysts*, vol. 13, p. 1079, July 2023.